The slow retraction method (SRM) for the determination of ultra-short relaxation times in capillary break-up extensional rheometry experiments

Laura Campo-Deaño, Christian Clasen*

Department of Chemical Engineering, Katholieke Universiteit Leuven, Willem de Croylaan 46, 3001 Heverlee, Belgium

Abstract

We monitor the capillary thinning and breakup of low viscous liquid filaments with high speed imaging to determine the relaxation time of dilute polymer solutions in extension. The induction of filament thinning by a slow extension of a liquid bridge beyond the static stability limit enables one to create axially symmetric thinning profiles with minimized inertial oscillations from acceleration of the liquid. The minimized disturbance of the capillary thinning process by this slow retraction method (SRM) allows the observation and quantitative fitting of the visco-capillary and inertio-visco-capillary balance as well as the potential flow regime for a series of Newtonian liquids covering a viscosity range from 350 to 27 mPa s. For dilute solutions of polyethylene oxide in water the SRM allows the reliable determination of relaxation times in extension of as low as 240 μs. A lower limit for the polymer concentration c_{low} below which an elasto-capillary balance cannot be observed is introduced, based on the finite extensibility limit L^2 of the

*Corresponding author. Tel: +32 16 3 22354; Fax: +32 16 3 22991
Email address: christian.clasen@cit.kuleuven.be (Christian Clasen)

polymer chain.

Keywords: Capillary thinning, Caber, extensional rheometer, static stability limit, elongational rheometry, dilute polymer solution, relaxation time, elasto-capillary balance, self-similarity, finite extensibility, critical concentration.

1. Introduction

The uniaxial extensional viscosity η_E is a fundamental material property of a fluid which characterizes the resistance of a material to an uniaxial stretching deformations. While for rheologically simple fluids this viscosity is directly related to the shear viscosity η via the Trouton ratio $\eta_E = 3\eta$, for complex (micro-structured) or viscoelastic fluids, this extensional viscosity can be a function of both the rate of deformation and the total strain accumulated. In particular the highly increased extensional viscosity of viscoelastic solutions in comparison to simple fluids of similar shear viscosity has a strong impact on operations as mixing, pumping, spraying, coating and general processing or transport operations. The strong increase of viscoelastic material functions in extensional flows has a particularly pronounced effect in dilute polymer solutions due to the unraveling and extension of the initially coiled polymeric molecules by the strong extensional flows, whereas a contribution of the polymer to the shear viscosity is negligible [1, 2, 3, 4, 5]. One flow type where the effects of dissolved polymers on the extensional flow becomes especially apparent is the thinning and breaking of liquid filaments, since this free-surface flow is readily observable. Already the pioneering work of Middleman [6] and Goldin et al. [7] have shown the dramatic effects of

minute amounts of high-molecular-weight additives on the breakup of fluid filaments. For the case of jets of dilute polymer solutions the elastic stresses generated affect the breakup length of the jet and the ensuing droplet size distribution [8, 9]. For a low viscous, dilute polymer solution dripping from a faucet, the presence of the polymer can dramatically extend the time to pinch off and inhibit the existence of satellite droplets [10, 4, 11].

A quantitative description of the effects of polymer additives on low viscosity dilute polymer solutions requires a precise determination of the actual material properties in an extensional flow and therefore experimental techniques that allow their reliable measurement at relevant deformation rates. While for higher viscosity systems techniques as the Meissner [12, 13] or Münstedt apparatus [14, 15] have been introduced already a while ago, generating and measuring purely extensional flows of lower viscous, mobile fluids has proven to be extremely difficult. Attempts have been made to do this via the determination of pressure drop in porous media [16], opposed jet devices [17], spin-line rheometers and two- and four-roll mills [18, 19]. First reliable mechanical studies of the state of stress of lower viscous liquids in a well-defined uniaxial flow field were made by Sridhar et al. [20] using the filament stretching device, but were still limited to viscosities > 1 Pa s [21]. Only recently the capillary breakup extensional rheometry (Caber) has been introduced, that determines extensional flow material functions directly from the thinning dynamics of a liquid filament [2, 22, 23]. A capillary break-up experiment creates an unstable fluid filament by imposing a rapid axial step-strain of prescribed magnitude to a small fluid element. The formed liquid filament is then allowed to thin under the action of surface tension until it

finally breaks. The decay of the necking sample is governed by a balance of viscous, elastic, gravitational and capillary forces. A capillary breakup experiment has therefore no active control over the uniaxial deformation rate that a filament experiences and is therefore often considered to be an 'indexer' rather then an actual rheometer. However, for several special cases the Caber experiment can deliver absolute material properties, as for example an extensional viscosity for a Newtonian liquid [24], the power law index of an extension thinning fluid [25, 26], a yield stress against a uniaxial deformation [27, 28], or the longest relaxation time in an extensional flow [29]. In particular the possibility to determine and compare the extensional relaxation time to the shear relaxation time has been the subject of in-depth investigations [30, 31, 32, 3, 19, 23, 33, 34, 5, 4, 35, 36]. But although the Caber technique enables one to investigate fluids with viscosities below the limiting value of the filament stretching technique of 1 Pa s, Rodd et al. [37] have shown that there is also for the Caber technique a lower viscosity limit which is for Newtonian systems at $\sim$ 70 mPa s. The main limitation from an experimental point of view arises from the difficulty to create a low viscous liquid filament fast enough so that the thinning dynamics can still be observed. In a general Caber experiment the liquid filament is created outgoing from a drop of the fluid confined between two parallel circular plates that are subsequently quickly separated to a desired separation distance. The necessary fast acceleration and deceleration of the liquid when performing this initial stretch to create a filament of a low-viscous liquid are inherently coupled with inertia induced oscillations of the end droplets adhered to the endplates and an axial asymmetric filament profile. The effect of these oscillations on

the thinning dynamics of the filament cannot ignored at low viscosity levels and prevent a quantitative evaluation of the thinning dynamics below the critical limit indicated by Rodd et al. [37]. Furthermore, the inertial effects present also a limit to the determination of a relaxation time λ with a Caber experiment. Although the stabilizing effect of the polymer lowers the accessible viscosities to $\sim$ 1 mPa s, Rodd et al. [37] gave an empirical lower limit for the relaxation time determination of $\sim$ 1 ms [37]. Recently Vadillo et al. [38] presented with the Trimaster a Caber type experimental setup utilizing high speed plate separations that allowed to reliably determine the thinning dynamics of dilute polymer solutions with viscosities down to 10 mPa s and that could detect breakup time delays caused by the polymer of order 5 ms. For even lower viscosities and relaxation times, detailed investigations of the breaking dynamics of liquid threads had so far to rely on simulation techniques. Recent results by Bath et al. [39] using the Oldroyd-B model, and Ardekani et al. [40] using the Giesekus model where able to model the breaking dynamics and satellite drop formation for filaments with relaxation times down to O(1 ms) and viscosities of O(1 mPa s). However, as correctly stated in [40], "the [experimental determination of extensional viscoelastic properties for these] very low viscosity and weakly elastic liquids ... is a particular challenge using traditional rheometers", and "filament stretching devices or Caber devices cannot be used to measure the tensile properties of such low-viscosity liquid(s) because of the rapid timescales for breakup".

Still, an experimental technique that could probe (aqueous) solutions with viscosities of order O(1 mPa s) to determine relaxation times in uniaxial extensional free surface flows at the sub-millisecond scale is highly de-

sirable, since applications as for example ink-jet printing or atomization of drug loaded formulations in medical or pharmaceutical applications operate at thinning velocities where sub-millisecond relaxation times are dominant [41, 42] and where the addition of traces of polymers is used to structure the breaking dynamics and size and occurrence of satellite droplets [43].

In this paper we present therefore with the slow retraction method (SRM) a modified usage protocol of the general Caber setup that enables the reliable determination of breakup time delays and relaxation times of order $O(200\ \mu\text{s})$ in aqueous systems with viscosities of $O(1$ mPa s). The paper is structured as follows:

In the Materials and Methods section the operating principle of the slow retraction method to create a liquid filament of a low viscous liquid is introduced. The second section focuses then on the thinning behaviour of low viscous, Newtonian liquids. The third section discusses the thinning dynamics of dilute aqueous polymer solutions and introduces the theoretical limits of the slow retraction method for the detection of sub-millisecond relaxation times.

2. Materials and Methods

2.1. Experimental Setup

The capillary thinning experiments were carried out using the plate separation drive unit of a Haake CaBER-1 extensional rheometer (Thermo Haake GmbH, Karlsruhe, Germany) in order to control the position and separation velocities of two circular parallel plates with selectable diameters D_p of 4, 6 and 8 mm. Fluid samples were carefully loaded between the plates using a

syringe to ensure the absence of trapped air bubbles in the sample as well as between the sample and the plates. During and after the controlled separation of the plates to a final distance the evolution of the thinning fluid filament forming between the plates was monitored with video imaging using a high speed camera (Photron Fastcam SA-2, Photron, San Diego CA, USA) with a 12X zoom lens and two 2X extensions (Navitar, Rochester NY, USA), together with a fiber optic backlight source as shown in Figure 1. Each experimental test was repeated at least four times in order to corroborate reproducibility.

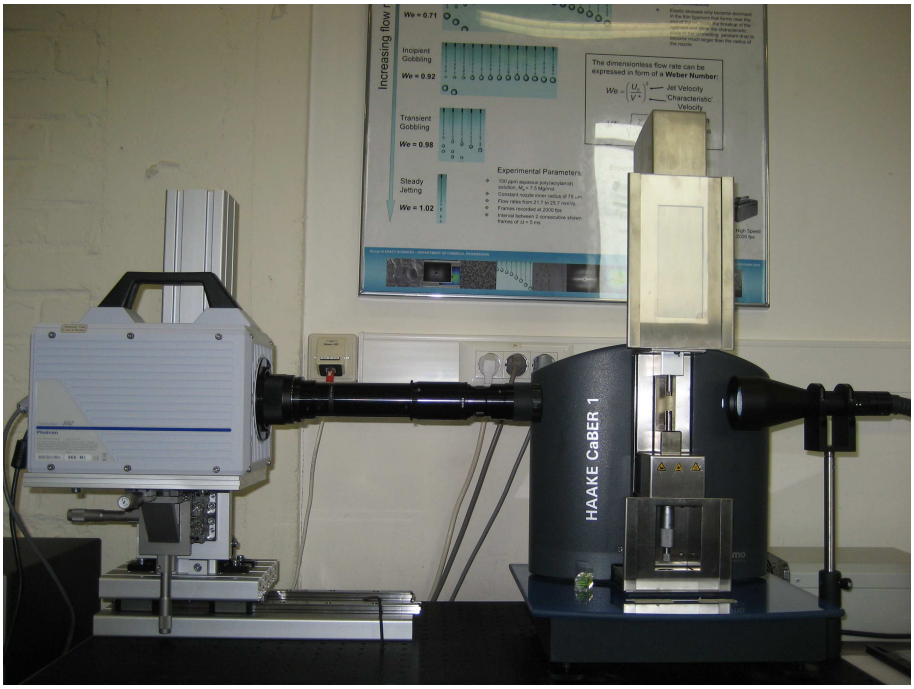

Figure 1: Experimental set up for the CaBER.

The video images were subsequently analyzed by digital image processing

in Matlab in order to determine the full filament profile and in particular the position and dimension of the minimum filament diameter D_{min}. In order to calibrate the diameters determined from the image processing, a series of standard diameter filaments (0.02, 0.03, 0.06, 0.12, 0.25, 0.50 and 1 mm) has been measured with the optical setup at the same experimental conditions. The correlation between the actual and observed diameters is given in Figure 2 and used for all subsequent investigations.

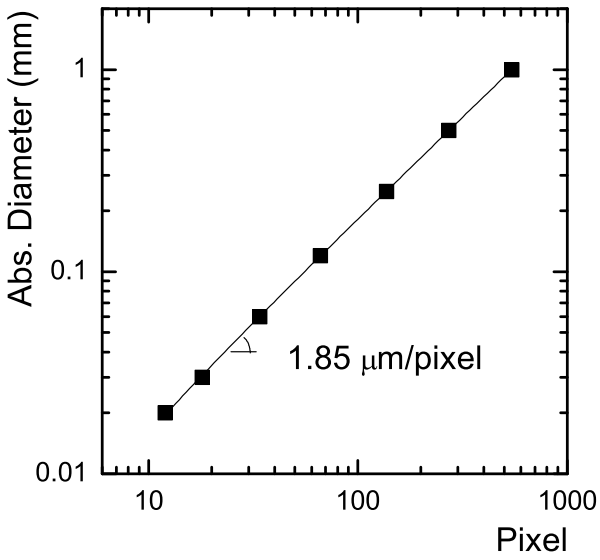

Figure 2: Millimeter to pixel ratio of the experimental setup, determined from images of fibers with absolute diameters of 0.02, 0.03, 0.06, 0.12, 0.25, 0.50 and 1 mm.

2.2. The slow retraction method (SRM)

For the creation of low viscous liquid filaments whose thinning dynamics are subsequently monitored we followed a procedure that is different from the general capillary breakup extensional rheometry (Caber) protocols. Start-

ing from the initial cylindrical liquid bridge with an initial aspect ratio of $\Lambda_0 = L_0/(2R_{mid}) = L_0/D_p$ (where L generally denotes the plate separation distance and R_{mid} the liquid bridge radius at $L/2$), the plates are separated with a moderate velocity of ~ 2 mm/s just slightly below a critical aspect ratio $\Lambda_{S,break}$ at which a statically stable liquid bridge (indicated by the suffix S) still exists.

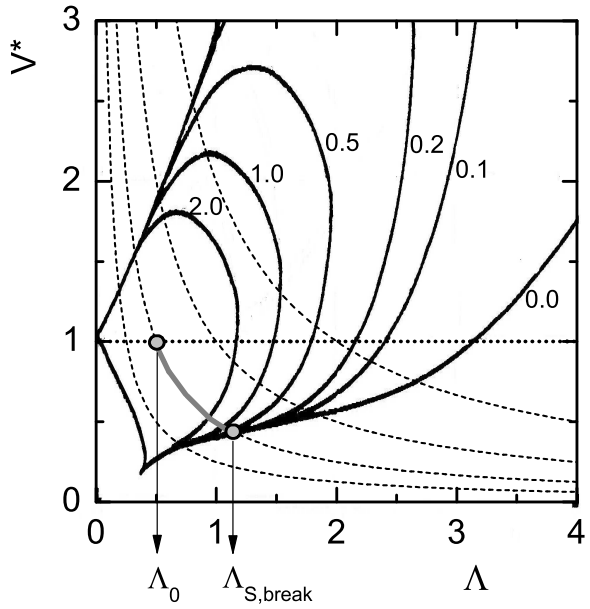

Figure 3: Critical volume stability limits $V*_{break}$ (solid lines, taken from [44]) as a function of the aspect ratio Λ for different Bond numbers Bo (indicated as numbers in the diagram). The dashed hyperbolas (eq. (1)) represent constant absolute fluid volumina. The dotted line indicates a cylindrical filament ($V^* = 1$). The indicated initial aspect ratio Λ_0 and the critical aspect ratio $\Lambda_{S,break}$ represent the values selected for measurements in the present paper

The critical aspect ratio of $\Lambda_{S,break}$ above which the liquid bridge becomes

unstable and collapses can be determined from the stability diagrams for liquid bridges of Slobozhanin et al. [44]. These diagrams give critical values of the dimensionless fluid volume

$$V^* = \frac{4V_0}{\pi D_p^2 L} \tag{1}$$

as a function of the aspect ratio Λ. Here V_0 refers to the total volume of the fluid which can be calculated from that of the initial cylindrical bridge as $(\pi D_p^2 L_0)/4$. The diagram in Figure 3 depicts (as solid lines) the critical volume stability limit V^*_{break} (beyond which the filament collapses) as a function of the aspect ratio Λ for different Bond numbers $B_0 = (\rho g D_p^2)/(4\gamma)$. The Bond number captures the effects of gravity against the surface tension and is a measure of how much the initial cylindrical filament 'sags'. Larger plate diameters D_p lead to more sagging and higher Bond numbers and therefore to critical volume stability limit curves V^*_{break} that reach there collapsing limit already at smaller critical aspect ratios $\Lambda_{S,break}$. Starting now for a filament breakup experiment in this diagram from a cylindrical configuration $V^* = 1$ (the dotted horizontal line) at Λ_0 and holding the total physical volume constant as the bridge is axially elongated by separating the plates, we follow the hyperbolic trajectory $V^* \sim L_0/L$ of eq. (1) (indicated as dashed lines). The axial elongation yields statically stable filaments until the hyperbola intersects the critical volume stability curve of the appropriate Bond number and enables one to extract $\Lambda_{S,break}$ from this intersection [27].

After reaching the stable separation distance just below $\Lambda_{S,break}$, a very slow separation velocity of the end plates of 0.11 mm/s was chosen in order to approach $\Lambda_{S,break}$ and initiate the filament breaking process which then

subsequently evolves on a timescale orders of magnitude faster than the slow plate separation speed . This 'slow retraction method' (SRM) assures that the effects of fluid inertia (that were inherent for a fast plate separation as described by Rodd et al. [37]) are minimized. Furthermore, in comparison to a fast initial separation, the slow retraction method leads to a a fully relaxed state of the liquid filament and its solution structure at the onset of the filament collapse [35]. The mid-filament radius R_{mid} at this point is denoted R_0 in the following. Figure 4 compares the breaking process of a 75% solution of glycerol in water, initiated with a fast separation (upper row) and with the slow retraction method (lower row of pictures). It can be seen that the oscillations in the end drops are strongly reduced with the slow retraction method and that the filament retains its axial symmetry to the final breaking point in comparison to the fast separation.

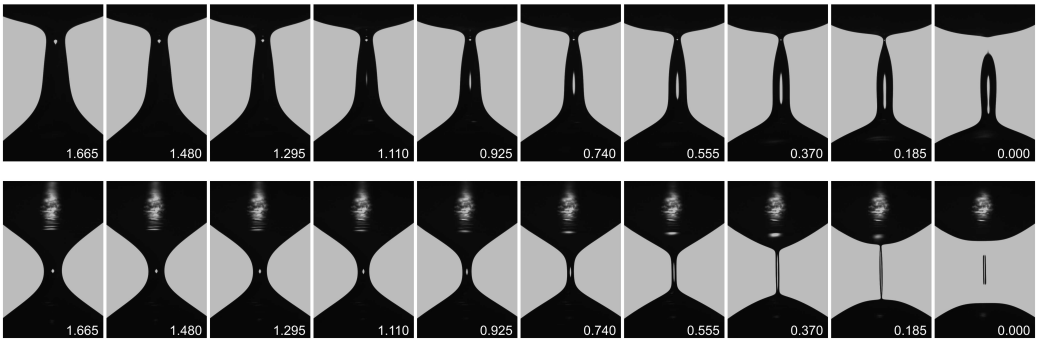

Figure 4: Comparison of the breaking dynamics induced by the slow retraction method (SRM) (bottom row) and by a fast separation (upper row) for a 75% glycerol/water mixture. The plate separation velocity of the SRM is 0.11 mm/s, and 170 mm/s for the fast separation method. The time to breakup is indicated in milliseconds on each consecutive picture. The plate diameter is $D_p = 4$ mm ($Bo = 0.648$).

In order to adjust the radius R_0 as well as the length of the collapsing filament, both the plate diameter D_p as well as the initial aspect ratio Λ_0 can be varied in order to affect the critical aspect ratio $\Lambda_{S,break}$ at which the filament will start to thin. We still follow the same hyperbolic trajectory in the stability diagram when keeping Λ_0 constant and increasing D_p. However, increasing D_p will lead to higher Bond numbers and therefore decreasing critical values $\Lambda_{S,break}$, but at same time increasing filament radii R_0. On the other hand, increasing the initial aspect ratio at constant plate diameter moves the hyperbola in Figure 3 away from the origin and therefore the intersect $\Lambda_{S,break}$ to larger aspect ratios. Both adjustments (increasing D_p at constant Λ_0, and increasing Λ_0 at constant D_p) will lead to longer thinning filaments at comparable radii, an effect that becomes important in the curvature discussion below. It should be noted that also Sattler et al. [11] have deliberately used $\Lambda_{S,break}$ as the final aspect ratio, however, with a fast initial separation to reach this limit.

2.3. Fluids

The Newtonian liquids used were aqueous solutions of glycerol (Acros Organics, Geel, Belgium) at different concentrations of 75, 85, 90 and 95 wt%. The shear viscosity was measured using a stress-controlled rheometer (AR-G2, TA Instruments) at 25^oC, and the surface tension γ was determined with a Wilhelmy plate method. The resulting values are shown in Table 1. As a non-Newtonian fluid, aqueous solutions of poly(ethylene oxide) (POLYOX Resin WSRN N-12K, Union Carbide) with a nominal mass average molecular weight of 1.000.000 g/mol and an equilibrium surface tension of $\gamma = 62$ mN/m [4] were used. Solutions in pure distilled water of 0.0005, 0.001, 0.002, 0.005,

0.01, 0.02 and 0.05 wt% of PEO were prepared at room temperature, and gently stirred for 24 h to speed dissolution.

Table 1: Shear viscosity η and surface tension γ for the glycerol in water solutions at 25^oC.

	η (mPa s)	γ (mN/m)
75%	27.0 ± 0.1	64.8 ± 1
85%	76.8 ± 0.1	64.0 ± 1
90%	149.9 ± 0.1	63.6 ± 1
95%	319.2 ± 0.1	63.0 ± 1

3. Results and Discussion

3.1. Newtonian Fluids

Before the next chapter focuses on the filament thinning behaviour of dilute polymer solutions and the determination of relaxation times from these experiments, it is necessary to first investigate the thinning dynamics of the pure (Newtonian) solvents to validate the slow retration method (SRM) and to determine the general effects that the SRM has on the breaking dynamics.

Figure 5 shows the last 4 milliseconds of filament thinning of the four glycerol solutions that span a range of viscosities from 27 to 320 mPa s at a surface tension of ∼64 mN/m (exact values in table 1). Each fluid was probed with 3 different plate diameters and 2 initial aspect ratios Λ_0. In order to follow the fast evolution of the filament diameter, a frame rate of 5400 frames per second was selected with a resolution of 256 x 832 pixels at 1.8 microns/pixel for the video imaging. In addition to the diameter

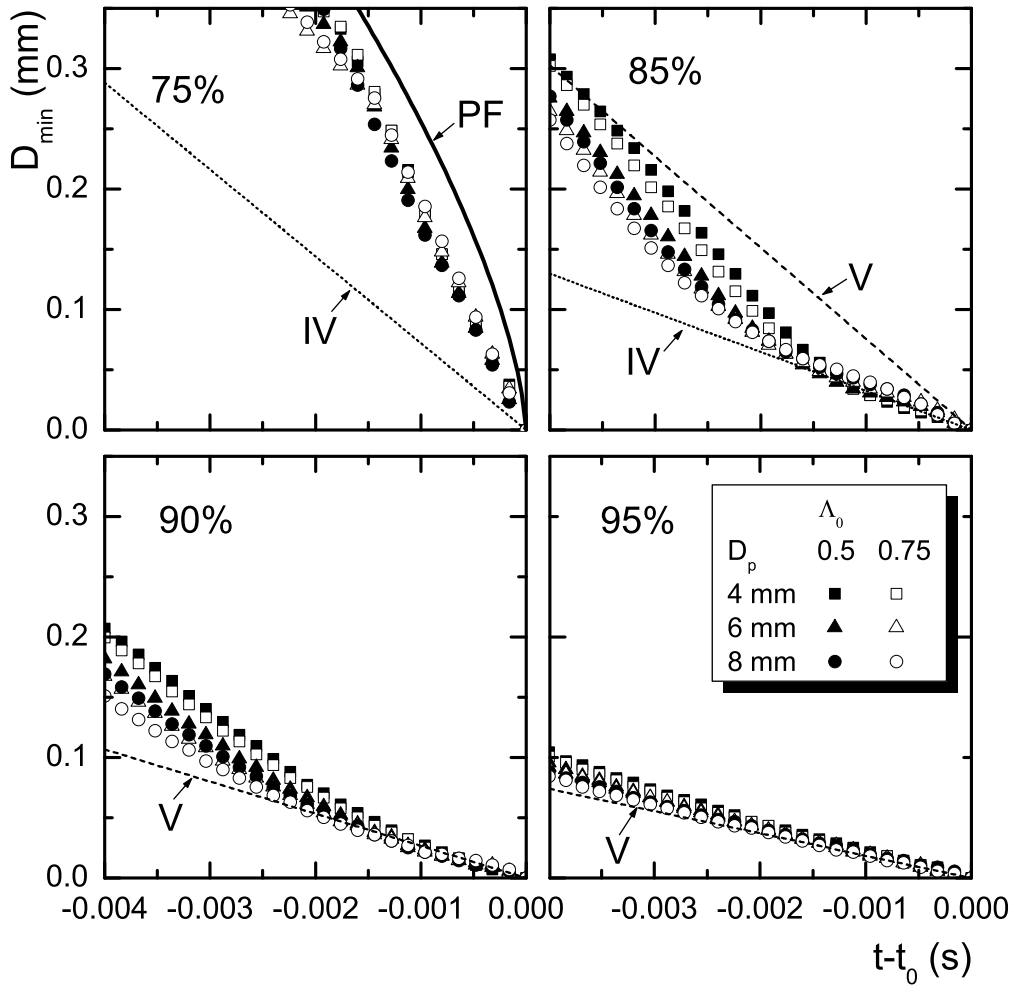

Figure 5: Time evolution of the minimum filament diameter D_{min} close to breakup for four concentrations of glycerol in water and for three different endplate diameters D_p and two initial aspect ratios Λ_0 as indicated in the legend, at 25^oC. Also shown are the calculated thinning curves for the visco-capillary balance (V-regime) of eq. (2) (dashed line), for the inertio-visco-capillary balance (IV-regime) of eq. (4) (dotted line), and for the PF regime of eq. (5) (solid line), using the the viscosity and surface tension of Table 1

.

evolution of Figure 5, Figure 6 gives for a plate diameter of $D_p = 4$ mm and an aspect ratio of $\Lambda_0 = 0.5$ for each concentration a series of images of the full filament shape with time intervals that directly relate to the data point spacing in Figure 5.

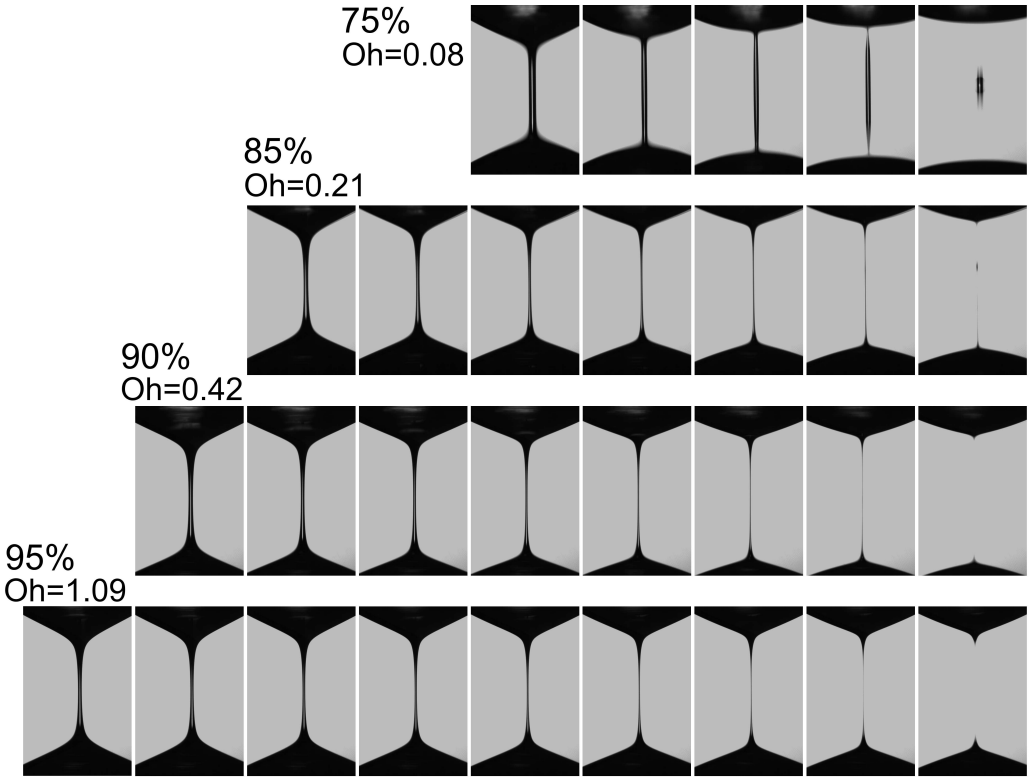

Figure 6: Thinning and pinch-off of the filament for solution of a) 75%, b) 85%, c) 90% and d) 95% of glycerol in water at 25^oC. The time interval between each consecutive picture amounts to 0.185 ms, the plate diameter D_p used was 4 mm with an initial height of 2 mm (initial aspect ratio $\Lambda_0 = 0.5$).

The thinning diagrams in Figure 5 represent four critical cases of the SRM when approaching the breaking behaviour of low viscosity fluids. For

the highest viscous solution in Figure 5 (95 wt% glycerol) the liquid filament decays linear with time prior to breakup and (as can be seen in Fig. 6) with a stationary minimum filament diameter and breaking point in the middle of the filament. This is expected, since for a sufficiently high viscosity the squeezing action of the capillary pressure is solely balanced by the viscous stresses in the filament. In this viscosity controlled thinning regime (in the following indicated as 'V' regime) the slender filament that develops close to breakup becomes independent of initial conditions and evolves in a self-similar way with the smallest diameter D_{min} and final breaking point in the middle of the filament. The minimum radius evolution can in this case be described by similarity solutions [45] of which the most stable one was found by Papageorgiou [46, 47]:

$$R_{min} = 0.0709\frac{\gamma}{\mu}(t_0 - t), \tag{2}$$

where t_0 is the time at filament breakup. The dashed line in Figure 5 for the concentration 95% gives the Papageorgiou solution of eq. (2), using the shear viscosity η and surface tension γ of Table 1.

For the solution of 90% Figure 5 shows that the final stages of thinning are still in the V regime and are well described by the indicated Papageorgiou solution (dashed line). However, the linear thinning regime is reached at later stages as compared to the 95% solution and we can clearly observe an accelerating thinning regime before the linear, viscosity controlled thinning sets in. The reason for this is that the Papageorgiou solution is only applicable for long, slender filaments with axial length scales much larger then radial. On the other hand, the slow retraction method as a tool to create

observable filaments is deliberately using the smallest possible final aspect ratio $\Lambda_{S,break}$ and therefore creating the shortest possible filaments with an inherently high axial curvature. The mean curvature κ of the filament surface can be described via [48]

$$\kappa = \frac{1}{R\left(1+(R')^2\right)^{0.5}} - \frac{R''}{\left(1+(R')^2\right)^{1.5}}, \tag{3}$$

where $R = R(z)$ is the radius of the filament along the axial or z-direction and $R' = dR/dz$ and $R'' = d^2R/dz^2$ are the respective first and second spatial derivatives. At the location of the minimum radius R_{min} the first derivative is $R' = 0$ and the second derivative reduces to the inverse of the radius R_z of the tangentially adjacent circle (indicated in Fig. 7), $R'' = 1/R_z$, so that the mean curvature of eq. (3) reduces at this point to $\kappa = 1/R_{min} - 1/R_z$. The apparent acceleration of the filament thinning originates then from the initially high value of $1/R_z$ that causes a lower mean curvature and therefore a lower Laplace pressure at the necking point in comparison to a slender filament of same radius R_{min}. During the thinning process $1/R_z$ becomes smaller, resulting in the apparent acceleration of the thinning until the mean curvature $\kappa = 1/R_{min} - 1/R_z$ approaches the radial curvature $1/R_{min}$ and the slender filament shape required for the applicability of the Papageorgiou solution is reached.

Comparing the ratio of mean curvature κ and radial curvature $1/R_{min}$ (shown in Figure 8 as the relative curvature κR_{min}) for representative thinning experiments of 95%, 90% and 85% glycerol solutions with the observable linear thinning range in Figure 5 enables one to determine a critical relative curvature, below which a slender filament is reached. This critical relative curvature is indicated in Figure 8 by the dotted line and equates to κR_{min}

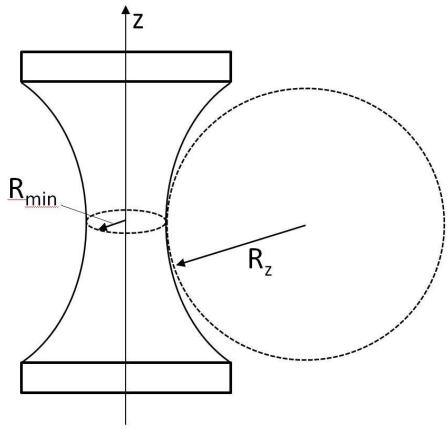

Figure 7: Schematic drawing of the filament radius R and the axial radius R_z.

= 1.006. This limit gives now a practical value to the general 'slenderness' requirement for the application of similarity solution and the range of radii where linear fits of $R_{min} \sim (t_0 - t)$ can be used to extract material properties from capillary thinning experiments.

The thinning curves of Figure 5 for 90% and 85% indicate that also the initial aspect ratio and plate diameter have an influence on when the critical relative curvature and a slender filament is reached when using the slow retraction method. As it can be seen in Figure 5, increasing the end-plate diameter from 4 to 8 mm at a constant initial aspect ratios Λ_0 shifts the onset of a clearly visible self similar thinning regime to earlier times. Also an increase of the initial aspect ratio at a constant plate diameter has the same effect. This is not unexpected as both cases increase the filament length and decrease therefore the axial curvature at comparable radii as discussed for the critical volume stability limit above.

However, both larger plate diameters and initial filling height lead to

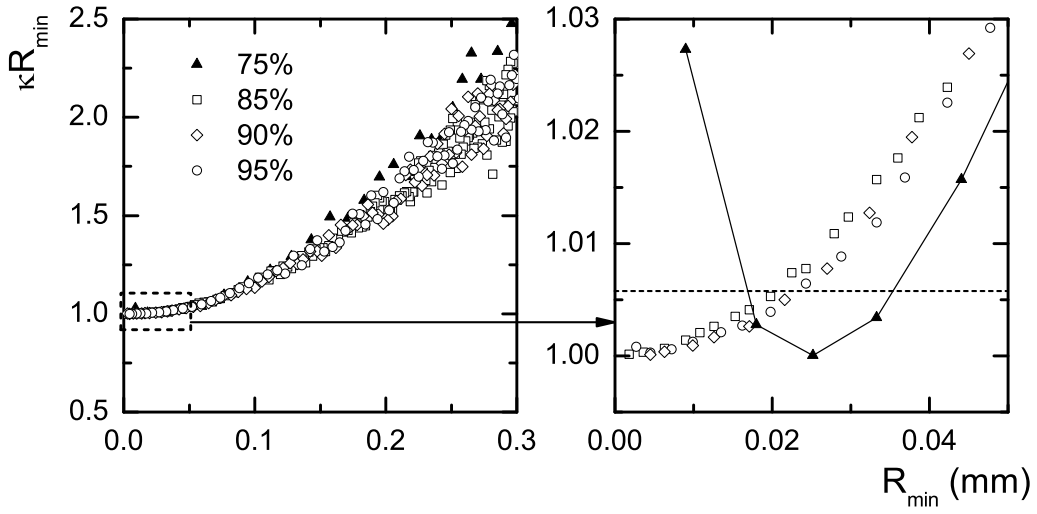

Figure 8: Ratio of the mean curvature κ to the radial curvature $1/R_{min}$ as a function of the minimum radius R_{min}. Data for R_z were obtained from tangential fits to the digitized filament profiles of Fig. 9 at the minimum of the radius $R(z)$. The dotted line marks the critical relative curvature κR_{min} below which the experimental data in Figure 5 follow the linear similarity solutions.

larger Bond numbers and therefore less reproducible results due to difficulties in achieving similar initial fillings of the gap. Optimal plate diameter and initial aspect ratio for a sufficient reproducibility of the data for the current investigation of low viscous solutions were $D_p = 4$ mm and $\Lambda_0 = 0.5$ which will be used throughout the following experiments and discussions.

The solution of 85% glycerol in Figure 5 marks then a transition in the thinning behaviour. While it is still possible to observe a linear thinning close to breakup, the images of Figure 6 reveal that the filament is not breaking in the middle anymore, but that the location of the minimum filament diameter D_{min} is shifting in axial direction towards the end drops. This becomes more

obvious in Figure 9 that depicts the digitized filament profiles of figure 6 with intervals of time of 0.185 ms (The location of the minimum radius R_{min} is for each profile indicated by the bold arrows where it deviates from the midfilament location $z = 0$).

In this case velocities in the filament become so large that inertia can no longer be neglected and the thinning behaviour prior to breakup is controlled by an inertio-visco-capillary balance (the so-called 'IV' regime). The similarity solution found by Eggers [49] that describes this IV thinning regime does not contain the fluid density and differs from the visco-capillary thinning (eq. 2) only by the front factor

$$R_{min} = 0.0304\frac{\gamma}{\mu}(t_0 - t). \tag{4}$$

However, the determination of the minimum filament radius requires in this case the evaluation of the full filament shape as the location of the minimum radius shifts away from the filament middle. A comparison of the thinning data of the 85% solution in Fig. 5 with the IV solution of eq. (4) (dotted line) shows good agreement.

For the 75% glycerol solution the shifting of the minimum filament diameter R_{min} away from the middle of the filament and the final breaking close to the enddrops becomes even more obvious in the pictures of Figure 6 as well as in the digitized profiles of Figure 9. However, fitting the minimum diameter data in Figure 5 with the IV solution of eq. (4) (dotted line) does not work anymore. The thinning data for the 75% solution is much closer to a purely inertia controlled thinning, indicated by the solid line in Figure 5. This thinning behaviour (the so called potential flow 'PF' regime), that

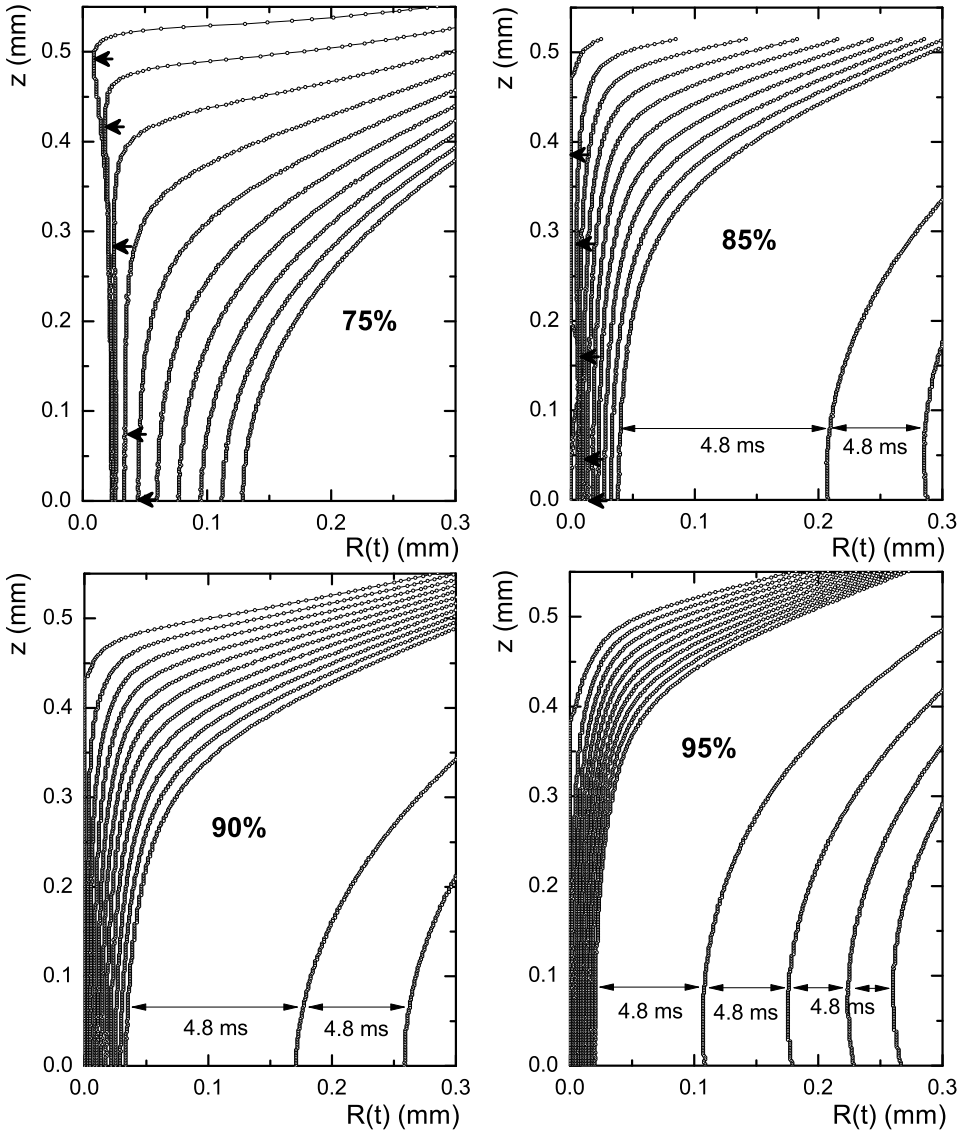

Figure 9: Time evolution of the filament profile $R(z)$ for the glycerol/water mixtures of Fig. 6 , at 25^oC. The time intervals between the profiles are 0.185 ms, larger time intervals are indicated in the graphs. Bold arrows indicate the position of the minimum radius R_{min} where this is not located at the mid-filament position $z = 0$.

is described by a power law as derived by [50, 37]

$$R_{min} = 0.64 \left(\frac{\gamma}{\rho}\right)^{\frac{1}{3}} (t_0 - t)^{\frac{2}{3}}, \tag{5}$$

is generally observed for low viscous fluids where the capillary pressure is only resisted by the inertia of the accelerating fluid molecules.

The experimental data of the 85% solution in Fig. 5 are actually for a similar glycerol concentration and viscosity as the numerical simulations by Chen et al. [51] and the experiments of Rothert et al. [52] that predicted and showed the existence of an IV thinning regime. The faster thinning data in Fig. 5 prior to the onset of the linear regime are, however, caused by the initially high axial curvature and lack of sufficient slenderness of the filament. We can therefore not judge if the thinning prior to the onset of the IV regime is following a V or PF scaling.

The general question, if the overall thinning dynamics of a filament are controlled by viscosity (as for the 95% and 90% glycerol solutions in Figs. 5, 6 and 9) or by inertia (the 85% and 75% glycerol solutions) can be answered by calculating the Ohnesorge number

$$Oh = \frac{\eta}{\sqrt{\rho \gamma R}}. \tag{6}$$

that compares the timescales of a viscosity controlled breakup $t_v = \eta R/\gamma$ and an inertia controlled breakup $t_\rho = 0.3413\sqrt{\rho R^3/\gamma}$ [37]. In order to determine the critical value of the Ohnesorge number below which a filament breakup will be controlled by inertia rather then the viscosity, one needs to compare the actual velocities with which the filament thins in the PF and in the V regime. Outgoing from eqs. (2) and (5) one can obtain via the

first derivatives the thinning velocities $U = -dR/dt$ as $U_\eta = 0.0709\gamma/\eta$ for the viscous thinning regime and $U_\rho = 0.3413\sqrt{\gamma/(\rho R)}$ for the potential flow regime. Formulating then a Ohnesorge number via the ratio of these velocities (rather than as a ratio of timescales as done in the derivation of Rodd et al. [37]) we obtain the appropriate numerical front factor that describes the correct transition value for the Ohnesorge number when $U_\rho = U_\eta$:

$$\frac{U_\rho}{U_\eta} = \frac{Oh}{0.2077}. \tag{7}$$

Using the initial radius of the cylindrical filament of R = 2 mm we obtain $Oh = 1.09$ for the 95% glycerol solution and $Oh = 0.08$ for the 75 % solution (Oh values are also indicated in the figure 6). The Ohnesorge number of $Oh = 0.21$ calculated for the solution of 85% that shows a breaking behaviour right at the transition between viscous and inertia control is then in excellent agreement with the the critical value of 0.2077 of eq. (7). Furthermore, the experimental results in Fig. 6 are also in good agreement with numerical calculations of the filament profiles for similar Ohnesorge numbers. A comparison to Fig. 1d and 3b in [39] shows for example that the predicted formation of the small bead on a string structure at $Oh = 0.4$ and $Oh = 0.2$ is actually observed in our experiments for the 75% solution at $Oh = 0.21$.

While the above classification via the Ohnesorge number allows a determination of the 'global' or overall breaking behaviour, Eggers [49] has shown that also during the thinning process any initially in the PF regime starting filament will eventually turn over to an IV thinning. The minimum filament radius at which this transition sets in can be determined from a local Ohnesorge number [53, 51, 27, 26]. Assuming that this transition takes

place when the length scale that enters the Ohnesorge number (the radius R_{min}) reaches a value so that the Ohnesorge number takes on the critical value $Oh^* = 0.2077$ of eq. (7), we can calculate the corresponding critical minimum filament radius at which this transition sets in:

$$R^* = 23.2\frac{\eta^2}{\rho\gamma}. \tag{8}$$

From a practical point of view the transition to the IV regime is done at $\sim 0.3Oh/0.2077$ [51] and the fully developed linear thinning regime can therefore be observed at $\sim 0.1R^*$. For the 85% glycerol solution with a viscosity of 77 mPa s this critical limit equates to $0.1R^* = 0.8$ mm and the linear IV thinning regime is therefore still within the observable limits in Figure 5. However, for the 75% solution with a viscosity of 27 mPa s, this transition radius calculates to $R^* = 0.26$ mm and the clear onset of linear IV thinning therefore to $0.1R^* = 0.026$ mm. From these radii follows that most of the thinning data observed in Figure 5 for the 75% solution is within the transitional regime between PF and IV thinning, and the onset of linear thinning is expected only at the last data point.

Since the viscosity enters eq. (8) squared, it becomes clear that for even lower viscosities also the critical radius R^* will leave the observable window. For aqueous systems with viscosities of 1 mPa s the critical radius R^* is of order $O(0.1\mu m)$ and the thinning dynamics in the observable diameter range will follow solely a PF thinning and eq. (5). In the following section, that focuses on the thinning dynamics of dilute aqueous polymer solutions, we will therefore observe only the PF thinning dynamics before the onset of any observable polymer contribution.

3.2. Dilute Polymer Solutions

In this section the filament thinning behaviour of a series of dilute aqueous solutions of polyethylene oxide with a molecular weight of 1.000.000 g/mol is investigated with the SRM. The solutions have a constant shear viscosity from 1 to 3 mPa s approximately, and will therefore show initially a thinning behaviour within the PF regime. For the capillary breakup experiments an initial aspect ratio of $\Lambda_0 = 0.5$ and plate diameter $D_p = 4$ mm were chosen as determined in the previous section for most reproducible results. In order to be able to observe short relaxation times in the inertial flow regime, a recording rate of 15000 frames per second was selected with a resolution of 256 x 320 square pixel and 1.8 μm/pixel.

In Figure 10 the evolution of the filament radius R_{min} with time is shown for the different PEO concentrations. For a better visualization the curves are shifted by a time t_p along the time axis so that the initial PF regimes collapse onto the pure solvent curve [4]. As it can be seen in Figure 10, the initial necking of all dilute polymer solutions is similar to the Newtonian solvent and following the PF thinning of eq. (5) (indicated by the solid line in Figure 10). The SRM assures that at the beginning of the thinning process the polymer molecules are unstretched and the capillary pressure is solely balanced by inertial acceleration in the fluid column. However, for high enough extension rates ($\dot{\epsilon}\ \lambda > 0.5$) the chains will eventually undergo a coil-stretch transition, start to unravel and begin to balance with their resulting entropic stresses the squeezing action of surface tension. In this case close to $t - t_p = 0$ a transition from the initial PF thinning regime to an elasto-capillary (EC) balance regime is observed and the necking fluid filament is formed into a

long thin thread that thins exponential with time. As indicated by the first three pictures in Figure 10, the minimum filament radius is initially moving towards the enddroplets as expected for a PF thinning. The thin filament that forms (stabilized by the unraveling polymer) is therefore for the lower polymer concentrations located on both sides between a large satellite drop in the middle and the two enddrops [39, 40] (in the following we have evaluated the evolution of the upper filament). Measurements of the thinning rate in the elastic thinning regime can be used to estimate the relaxation time λ for the polymer solution in an extensional flow. As long as the finite extensibility limit of the molecules is not yet reached the balance between elastic stresses and capillary pressure results in an exponential decrease in the filament radius, with a time constant corresponding to three times the longest relaxation time of the fluid [29, 23, 54]

$$\frac{R_{min}}{R_0} = \left(\frac{GR_0}{2\gamma}\right)^{1/3} e^{\frac{-t}{3\lambda}}. \tag{9}$$

This exponential behaviour is clearly observed in the semi-log presentation of Figure 10 for the highest concentrated solution of 0.05%, indicated by the straight fit line. Also for 0.02 and 0.01% this exponential decay is clearly visible after an initial disturbance of an inertio elastic wave at the transition from the PF to the EC thinning regime. The values for the respective relaxation times obtained from the fits of eq. (9) are given in Table 2. These relaxation times determined with the slow retraction method are with 0.24 ms the lowest reliably reported so far for capillary thinning experiments, and below the limit of 1 ms indicated by Rodd et al. [37].

The exponentially thinning filament in the EC regime develops prior to

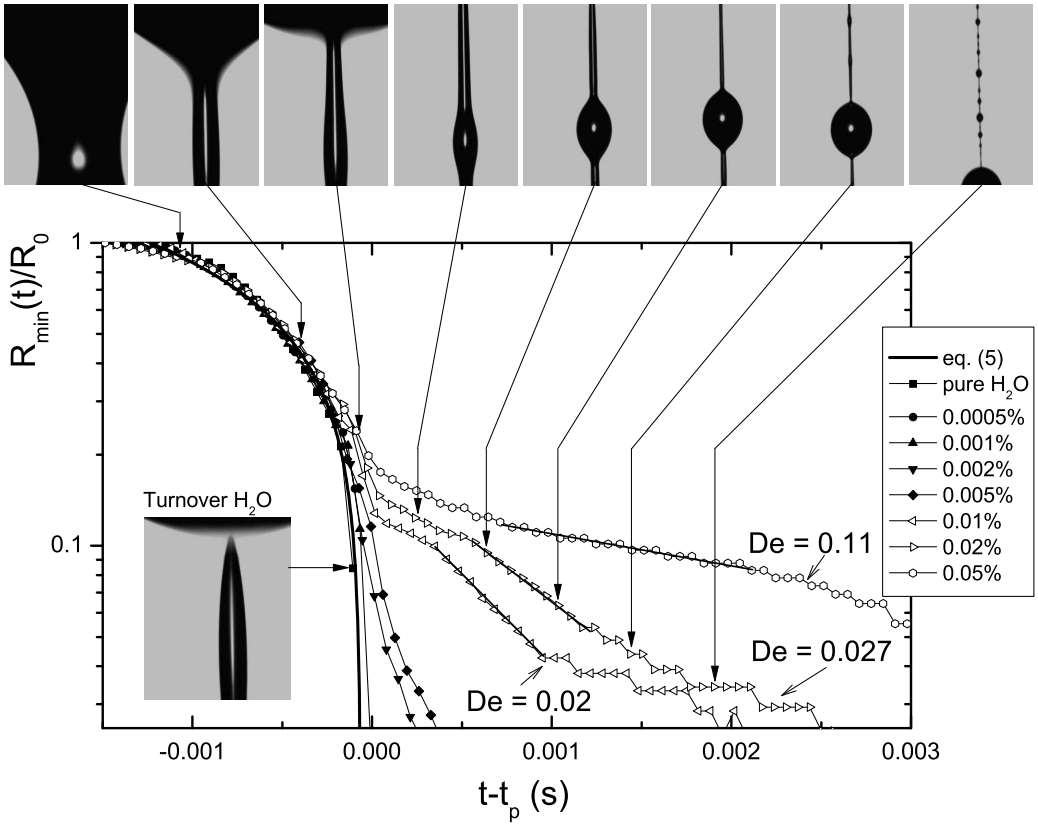

Figure 10: Time evolution of filament diameter for the different PEO concentrations, at 25^oC. The straight lines on the three highest concentrations represent exponential fits following eq. (9).

breakup further instabilities that can be observed as the 'bead-on string' structure in the last pictures of Figure 10 [54, 55]. Although the evaluation of an exponential thinning regime is, in principle, also possible from the string between the higher order generations of beads [56, 40], the induced oscillations by the occurrence of the higher order satellites [40] induces too much noise for a quantitative evaluation of the radius data and we restricted

Table 2: Relaxation times from capillary break-up experiments and Zimm relaxation times for the aqueous PEO solutions.

	λ (ms)	λ_Z (ms)
0.05%	1.38	0.107
0.02%	0.322	0.107
0.01%	0.240	0.107
0.005%	-	0.107
0.002%	-	0.107

the fit to obtain the relaxation time to the thinning regime before the onset of the bead-on-string structure.

The experimentally observed diameter evolutions in Figure 10 are very similar to the predictions of numerical simulations of [39] for low viscous and weakly elastic polymer solutions. Calculating the respective Deborah numbers $De = \lambda/\sqrt{\rho R^3/\gamma}$ from the accessible relaxation times λ in Table 2 and the initial radius of $R = 2$ mm (indicated in Figure 10), we can compare the experimentally observed breaking behaviour in Fig. 10 to the simulations in Fig. 3a of [39]. It is obvious that for both a Deborah number of $De = 0.02$ as well as $De = 0.1$ the experiments confirm the radius evolution predicted by the simulations, in particular the figure sequence in Figure 10 for $De = 0.027$ reflects the simulated profiles of Fig. 3b(Bottom) in [39] for $De = 0.02$.

3.3. Lower concentration limit for the determination of a relaxation time

One could also be tempted to perform an exponential fit on the thinning data of the lower concentrations of 0.005 % and 0.002%. However, the capability of a capillary breakup experiment to extract a relaxation time from

the thinning data is limited to a critical minimum concentration. As laid out by Clasen et al. [5], for higher viscosity solutions a lower limit of the visible effects of the polymer concentration on the thinning dynamics is reached when even the fully unraveled polymer chains will carry less stress than the solvent. This can be related to the lower viscosity solutions in this paper when looking again at the Ohnesorge number of eq. (6). The viscosity η that enters the Ohnesorge number for a dilute polymer solution consists of a contribution of the solvent and of the polymer $\eta = \eta_s + \eta_p$. For a low viscous solvent in an extensional flow the solvent contribution η_s is negligible and the viscosity originates primarily from the viscosity contribution η_p of the unraveling polymer chains. Following a FENE model description of the polymer stress in a dilute solution in an uniaxial flow, the stress originating from the polymer coils can be described as GA_{zz}, where

$$G = nkT = \frac{cN_A k_B T}{M_w} \tag{10}$$

is the modulus of the polymer in solution (with N_A and k_B as the Avogadro and Boltzman constants respectively), and A_{zz} is the axial component of the conformation tensor $\mathbf{A}$ (defined as the ensemble average second moment configuration tensor of the entire chain, $\mathbf{A} = \frac{<\mathbf{QQ}>}{Q_{eq}^2/3}$, normalized with the equilibrium coil end-to-end distance Q_{eq}). The polymer contribution to the extensional viscosity $\eta_p = GA_{zz}/\dot{\epsilon}$ reaches its maximum when the polymer chains approach their finite extensibility limit where $A_{zz} \sim L^2$ and the extensional viscosity reduces to the constant value $2G\lambda L^2$ [5] (here L^2 denotes in FENE terminology the finite extensibility limit of the polymer coils that is defined as the trace of the conformation tensor of the polymer coil,

$tr\mathbf{A}$, at full stretch). With these assumptions the local Ohnesorge number reduces at the finite extensibility limit to [57]

$$Oh = \frac{2G\lambda L^2}{3\sqrt{\rho\gamma R}}. \tag{11}$$

For a given modulus G (or concentration c via eq. (10)) this equation can be solved for a critical radius R_{Oh} at which the initial PF thinning changes to a V thinning regime controlled by the constant viscosity of the fully unraveled polymer chains:

$$R_{Oh} = 23.18\frac{\left(\frac{2}{3}G\lambda L^2\right)^2}{\rho\gamma}. \tag{12}$$

The numerical front factor arises from the critical value for the Ohnesorge number $Oh = 0.2077$ from eq. (7). This radius R_{Oh} at which this transition from the PF to the V regime is observed decreases with decreasing polymer concentration and eventually leaves the observation window.

However, the above assumption of fully unraveled polymer coils can lead to an overestimation of this critical radius, since the polymer coils first have to unravel during the thinning process in order to reach the finite extensibility limit. The onset of unraveling will not occur at the initial filament radius R_0, but only when the extension rate $\dot{\epsilon} = -(2/R)(dR/dt)$ in the thinning filament overcomes the critical limit $\dot{\epsilon}\lambda = 0.5$ that marks the coil-stretch transition of a polymer. Using the extension rate $\dot{\epsilon}_\rho$ for an inertia controlled filament thinning (retaining the numerical factor of eq. (5) obtained from the similarity solutions for inertio-capillary breakup [37])

$$\dot{\epsilon}_\rho = 0.68\sqrt{\frac{\gamma}{\rho R^3}} \tag{13}$$

we can solve for the critical filament radius $R_{0,c}$ at which the coil-stretch transition will begin

$$R_{0,c} = 1.23 \left(\frac{\gamma \lambda^2}{\rho} \right)^{\frac{1}{3}}. \tag{14}$$

Assuming an affine deformation of the unraveling polymer chain with the fast elongating filament, the axial component of the conformation tensor $\mathbf{A}$ evolves with the radius as $A_{zz}R^4 = A_{zz,0}R_{0,c}^4$ [58] (The assumption of an affine polymer deformation is justified by recognizing that at $R_{0,c}$ a local intrinsic Deborah number that compares the inertia controlled time to break t_ρ with the relaxation time λ of the polymer [27] calculates to $De_0 = t_\rho/\lambda = (\gamma\lambda^2/(\rho R_{0,c}))^{0.5} = 0.73$. So for any instant happening at $t < t_\rho(R_{0,c})$ (e.g. the transition to an EC balance, or the polymers reaching their finite extensibility) the polymer relaxation can be neglected). An advantage of the SRM in order to create the thinning filament is now that the polymer coil will be initially in a relaxed state and therefore $A_{zz,0} = 1$ at $R = R_{0,c}$. In this case we can relate the filament radius R to the state of deformation of the polymer A_{zz} via

$$R = \frac{R_{0,c}}{A_{zz}^{\frac{1}{4}}} \tag{15}$$

The radius R_{L^2}, at which the polymer coils approach their finite extensibility limit so that one can assume $A_{zz} \sim L^2$ is then

$$R_{L^2} = \frac{R_{0,c}}{L^{\frac{1}{2}}}. \tag{16}$$

Only if the radius R_{Oh} (eq. (12)) at which the critical Ohnesorge number is reached is below this critical filament radius R_{L^2} we will observe a transition

from the PF to a V regime controlled by the viscosity $2G\lambda L^2$ of the already fully extended chains.

If the stresses that originate from the unraveling polymer coils become sufficiently large to balance the surface pressure before R_{L^2} is reached, we will observe a transition from the initial PF regime to an elasto-capillary (EC) balance during which the polymer chains are still further unraveling and have not reached their finite extensibility limit yet. Only in this EC regime is it possible to obtain via eq. (9) a relaxation time λ from the thinning dynamics.

However, the polymer concentration needs to be sufficiently high in order create enough polymers stress to stabilize an EC balance before the finite extensibility limit at R_{min} is reached. Similar to [5] a critical minimum polymer concentration c_{min} can be defined at the point where at least half the surface pressure is balanced by the stresses originating from the stretching polymers. With the polymer stress equal to GA_{zz} this condition is met when

$$\frac{\gamma}{R} = 2GA_{zz} \tag{17}$$

Combining this criterion with eq. (15) gives then the relation between a modulus (or concentration) and a critical radius R_{EC} at which the polymer stresses start to dominate the thinning dynamics and would show a transition to an elasto-capillary balance

$$R_{EC} = R_{0,c}\left(\frac{2GR_{0,c}}{\gamma}\right)^{\frac{1}{3}} \tag{18}$$

Setting the critical radii R_{L^2} and R_{EC} of eqs. (16) and (18) equal gives then the lower limit for the modulus G_{low} at which an observable onset of a polymer contribution to the thinning dynamics coincides with the polymer

just having reached its finite extensibility limit

$$G_{low} = \frac{\gamma}{2L^{\frac{3}{2}}R_{0,c}}. \tag{19}$$

The observation of an exponential thinning regime required for the determination of a relaxation time with eq. (9) from a Caber experiment is therefore not possible for a modulus below G_{low} or a concentration below the related critical concentration c_{low}. This critical concentration limit is larger than the minimum concentration c_{min} derived in [5]. While c_{min} in [5] gives the critical concentration below which the polymer will not affect the thinning dynamics and delay the breaking process, c_{low} indicates the (higher) concentration where the polymer will not only delay the breaking process, but where also the finite extensibility limit is not yet approached and a true exponential thinning regime following eq. (9) can be observed.

Still, the lower limit of the modulus G_{low} is just an order of magnitude estimation for two reasons. First of all, the relaxation time λ that enters eq. (19) via the critical radius $R_{0,c}$ (eq. (14)) is not known *a priori*. An estimate of λ for dilute solutions with the Zimm relaxation time λ_Z (eq. 21) (as done below) is going to underestimate λ. Even the lowest relaxation times in Table 2 that could be reliably determined from the exponential thinning profile in the capillary breakup experiments of Fig. 10 are roughly an order of magnitude larger than the Zimm relaxation time λ_Z. Using the Zimm time as an estimate in eq. (14) will therefore lead to an overestimation of G_{low} by a factor of ~ 5. Secondly, the stretching polymer chains will leave their linear response regime much earlier than at their finite extensibility limit. In [58] a linear response regime was estimated to hold until polymer

stretches of $A_{zz} = 0.1L^2$. Neglecting this criterion when calculating G_{low} leads therefore to an underestimation by a factor of ~ 5. Since both these effects work in opposite direction and by roughly the same factor, eq. (19) gives still a good order of magnitude estimation of the lower limit of the modulus. This can readily be seen when calculating the absolute lower limit for the concentration, c_{low}, by combining eqs. (10), (14) and (19)

$$c_{low} = \frac{1}{2.46} \frac{M_w}{N_A k_B T} \left(\frac{\gamma^2 \rho}{\lambda^2} \right)^{\frac{1}{3}} \frac{1}{L^{\frac{3}{2}}}. \tag{20}$$

An estimate for the relaxation time λ can be done with the Zimm time λ_Z [5]

$$\lambda_Z = \frac{1}{U_{\eta\tau}} \frac{[\eta]\eta_s M_w}{N_A k_B T}. \tag{21}$$

The universal ratio $U_{\eta\tau}$ [59] can be estimated from the excluded volume exponent ν as described by [4] via $U_{\eta\tau} = \zeta(3\nu)$ with ζ as the Riemann zeta function. For $\nu = 0.55$ for PEO in aqueous solution [4] $U_{\eta\tau}$ calculates to 0.463. The intrinsic viscosity $[\eta]$ can be calculated from the appropriate Mark-Houwink-Sakurada equation which is tabulated for the present system in [60] as $[\eta] = 0.072 M_w^{3\nu-1}$. With this we obtain for the Zimm relaxation time $\lambda_Z = 0.107$ ms. The finite extensibility parameter L^2 can be obtained from molecular parameters as the CC bond angle θ, the number of bonds j in a monomer unit with molar mass M_u and the characteristic ratio C_∞ for a given polymer [5]

$$L^2 = \frac{3}{k_\alpha^2} \left[\frac{j \sin^2(\theta/2) M_w}{C_\infty M_u} \right]^{2(1-\nu)}. \tag{22}$$

C_∞ is reported in [60] as 4.8 for $j = 3$ and an averaged bond angle θ in the PEO monomer unit taken as the CC bond angle. The additionally introduced swelling ratio k_α^2 that takes into account the polymer coil expansion in the relatively good solvent can be estimated by from the excluded volume exponent $k_\alpha^2 \approx \zeta(3\nu)/\zeta(1.5)$ [61] and equates for the current system to $k_\alpha^2 = 0.829$. With this the finite extensibility parameter calculates to $L^2 = 13713$ and we can now obtain the lower limit for the concentration from eq. (20) as $c_{low} = 0.009\%$.

This calculated value is in good agreement with the experimental data in Figure 10. For a concentration of $c = 0.01\%$ and all higher concentrations (open symbols) that are above the calculated critical value c_{low} a sufficiently long exponential thinning regime is clearly detectable. For the next smaller concentration of $c = 0.005\%$ (indicated by filled symbols) that is already below the calculated lower limit we can still observe an influence of the polymer on the breaking behaviour and a delayed breaking in comparison to the pure solvent. However, a clear exponential thinning regime is not observed. It might be tempting to do an exponential fit to the thinning data for the concentration $c = 0.005\%$ (and also for $c = 0.002\%$) that still show a delayed breakup time, in order to extract a relaxation time. However, outgoing from our analysis the thinning data will already be in the finite extensibility limit of the polymer and the apparent relaxation time will be shorter than the actual one. We attribute in the literature reported experimental relaxation times below the Zimm time to attempts to fit the thinning data of concentrations below the critical limit c_{low}.

For the lowest experimental polymer concentrations of $c = 0.001\%$ and

$c = 0.0005\%$ a calculation of the radius R_{EC} from eq. (18) at which an onset of a delayed thinning caused by the polymer can be expected yields values that are below the observable window in Fig. 10. And indeed, we do not observe a deviation from the thinning dynamics of the pure solvent in Fig. 10 for $c = 0.001\%$ and $c = 0.0005\%$. Furthermore, for these dilutions as well as for the pure solvent the minimum filament diameter is eventually located within an indention of the terminal drop, so that the 2-dimensional projection of the filament profile does not allow to observe the thinning dynamics beyond this so called 'turnover' point (indicated in Figure 10 for the case of pure water).

4. Conclusions

Conducting a capillary breakup experiment with the initial liquid bridge close to the critical aspect ratio $\Lambda_{S,break}$ of a statically stable state enables one to quantitatively investigate the thinning dynamics of low viscosity liquids. Using a slow retraction of the endplates that confine the liquid bridge in order to overcome the critical value of $\Lambda_{S,break}$ induces an axially symmetric thinning and minimizes effects of inertia induced oscillations of the end drops and the connecting filament. This slow retraction method allowed to follow the thinning dynamics of a series of Newtonian glycerol in water solutions with viscosities that span a range of 350 - 27 mPa s. The transition between a viscosity and an inertia controlled thinning, in particular the radius of the filament at which this transition takes place can be obtained from a local Ohnesorge number Oh (eq. (6)) that uses the radius $R_{min}(t)$ as the critical length scale. The numerical value for Oh at the transition could obtained

from a balance of the thinning velocities in the viscous (V) flow regime and the inertial (PF) flow regime to $Oh = 0.2077$. Equating the the critical radius of the transition from this local Ohnesorge number shows that the onset of the V regime shifts with decreasing viscosity to lower filament radii in accordance with the experimental observations for the glycerol solutions. The thinning dynamics allow for a clear observation of a V thinning regime for viscosities of 320 and 150 mPa s and a IV thinning for 77 mPa s. However, the SRM leads for Newtonian liquids to a high axial curvatures of the thinning filament, so that an evaluation of the thinning data with the similarity solutions of eqs. (2) and (4) is only possible for small radii where the mean curvature $\kappa = 1/R_{min} - 1/R_z$ approaches the radial curvature $1/R_{min}$. A practical value for the general 'slenderness' requirement for the application of similarity solution and the range of radii where linear fits of $R_{min} \sim (t_0 - t)$ can be used to extract material properties from capillary thinning experiments has shown to be $\kappa R_{min} = 1.006$.

For dilute polymer solutions with a shear viscosity of O(1 mPa s) the initial thinning dynamics of a liquid bridge (for which the endplate separation crosses the critical aspect ratio $\Lambda_{S,break}$) follow the PF thinning law of eq. (5). However, as soon as the unraveling polymer chains carry more stress then the surrounding solvent, the thinning dynamics switch over to an EC type thinning and allow to extract a relaxation time via eq. (9). Due to the initial PF thinning with local minimum radii close to the enddrops one observes two cylindrical filaments stabilized by the EC balance, with a large satellite drop in the middle. The observability of an EC thinning of the cylindrical filaments is limited by a critical concentration c_{low} of the poly-

mer. If the unraveling polymer chains reach their finite extensibility limit (at a concentration independent filament radius R_{L^2} (eq. (16))) *before* the polymer stress becomes sufficiently large to balance the capillary pressure (at a concentration dependent filament radius R_{EC} (eq. (18))) the EC balance will not be observable. Setting R_{L^2} and R_{EC} equal allows therefore to determine a lower limit for the modulus, G_{low} (eq. (19)) (or concentration c_{low}), below which a capillary breakup experiment will not allow the extraction of the relaxation time. Accounting for this concentration limit (which could be calculated for the investigated solutions of polystyrene in DEP to $c_{low} = 0.009$ %) a reliable relaxation time in extension as low as 240 μs at a concentration of 0.01% PEO could be determined with the SRM.

Acknowledgments

The authors would like to acknowledge financial support from the ERC starting grant 203043 NANOFIB.

References

[1] V. M. Entov, A. L. Yarin, Influence of elastic stresses on the capillary breakup of jets of dilute polymer solutions, Fluid Dynamics 19 (1984) 21–29.

[2] A. V. Bazilevsky, V. M. Entov, A. N. Rozhkov, Breakup of an Oldroyd liquid bridge as a method for testing the rheological properties of polymer solutions, Polymer Science 43 (2001) 716.

[3] M. Stelter, G. Brenn, A. L. Yarin, R. P. Singh, F. Durst, Investigation of the elongation behavior of polymer solutions by means of an elongational rheometer, Journal of Rheology 46 (2002) 507.

[4] V. Tirtaatmadja, G. H. McKinley, J. J. Cooper-White, Drop formation and breakup of low viscosity elastic fluids: Effects of molecular weight and concentration, Physics of Fluids 18 (2006) 043101.

[5] C. Clasen, J. P. Plog, W. M. Kulicke, M. Owens, C. Macosko, L. E. Scriven, M. Verani, G. H. McKinley, How dilute are dilute solutions in extensional flows?, Journal of Rheology 50 (2006) 849–881.

[6] S. Middleman, Stability of a viscoelastic jet, Chemical Engineering Science 20 (1965) 1037–1040.

[7] M. Goldin, J. Yerushalmi, R. Pfeffer, R. Shinnar, Breakup of a laminar capillary jet of a viscoelastic fluid, Journal of Fluid Mechanics 38 (1969) 689–711.

[8] D. W. Bousfield, R. Keunings, G. Marrucci, M. M. Denn, Nonlinear analysis of the surface tension driven breakup of viscoelastic filaments, Journal of Fluid Mechanics 21 (1986) 79–97.

[9] Y. Christanti, L. M. Walker, Surface tension driven jet break up of strain-hardening polymer solutions, Journal of Non-Newtonian Fluid Mechanics 100 (2001) 9–26.

[10] Y. Amarouchene, D. Bonn, J. Meunier, H. Kellay, Inhibition of the finite-time singularity during drop fission of a polymeric fluid, Physical Review Letters 86 (2001) 3558.

[11] R. Sattler, C. Wagner, J. Eggers, Blistering pattern and formation of nanofibers in capillary thinning of polymer solutions, Physical Review Letters 100 (2008) 164502.

[12] J. Meissner, Development of an uniaxial extensional rheometer for uniaxial extension of polymer melts, Transactions of the Society of Rheology 16 (1972) 405.

[13] J. Meissner, J. Hostettler, A new elongational rheometer for polymer melts and other highly viscoelastic liquids, Rheologica Acta 33 (1994) 1–21.

[14] H. Münstedt, New universal extensional rheometer for polymer melts - measurements on a polystyrene sample, Journal of Rheology 23 (1979) 421–436.

[15] H. Münstedt, S. Kurzbeck, L. Egersdörfer, Influence of molecular structure on rheological properties of polyethylenes. ii. elongational behavior, Rheologica Acta 37 (1998) 21–29.

[16] R. Haas, W. M. Kulicke, Flow behavior of dilute polyacrylamide solutions through porous-media. 2. Indirect determination of extremely high molecular-weights and some aspects of viscosity decrease over long-time intervals, Industrial and Engineering Chemistry Fundamentals 23 (1984) 316–319.

[17] G. G. Fuller, C. A. Cathey, B. Hubbard, B. E. Zebrowski, Extensional viscosity measurements for low-viscosity fluids, Journal of Rheology 31 (1987) 235–249.

[18] G. M. Harrison, J. Remmelgas, L. G. Leal, Comparison of dumbell-based theory and experiment for a dilute polymer solution in a corotating two-roll mill, Journal of Rheology 43 (1999) 197–218.

[19] S. L. Anna, G. McKinley, D. A. Nguyen, T. Sridhar, S. J. Muller, J. Huang, D. F. James, An interlaboratory comparison of measurements from filament-stretching rheometers using common test fluids, Journal of Rheology 45 (2001) 83–114.

[20] T. Sridhar, V. Tirtaatmadja, D. A. Nguyen, R. K. Gupta, Measurement of extensional viscosity of polymer-solutions, Journal of Non-Newtonian Fluid Mechanics 40 (1991) 271–280.

[21] G. H. McKinley, T. Sridhar, Filament-stretching rheometry of complex fluids, Annual Review of Fluids Mechanics 34 (2002) 375–415.

[22] A. V. Bazilevsky, V. M. Entov, A. N. Rozhkov, Liquid filament microrheometer and some of its applications, Third European Rheology Conference, D.R. Oliver (ed.), Elsevier Applied Science., 1990.

[23] S. L. Anna, G. H. McKinley, Elasto Capillary Thinning and Breakup of Model Elastic Liquids, Journal of Rheology 45 (2001) 115–138.

[24] G. H. McKinley, A. Tripathi, How to extract the Newtonian viscosity from capillary breakup measurements in a filament rheometer, Journal of Rheology 44 (2000) 653–671.

[25] P. Doshi, R. Suryo, O. E. Yildirim, G. H. McKinley, O. A. Basaran, Scaling in pinch-off of generalized Newtonian fluids, Journal of Non-Newtonian Fluid Mechanics 113 (2003) 1–27.

[26] R. Suryo, O. A. Basaran, Local dynamics during pinch-off of liquid threads of power law fluids: Scaling analysis and self-similarity, Journal of Non-Newtonian Fluid Mechanics 138 (2006) 134–160.

[27] G. H. McKinley, Visco-elasto-capillary thinning and break-up of complex fluids, Rheology Reviews (2005) 1–48.

[28] K. Niedzwiedz, O. Arnolds, N. Willenbacher, R. Brummer, How to characterize yield stress fluids with capillary breakup extensional rheometry (caber)?, Applied Rheology 19 (2009) 10.

[29] V. M. Entov, E. J. Hinch, Effect of a spectrum of relaxation times on the capillary thinning of a filament of elastic fluids, Journal of Non-Newtonian Fluid Mechanics 72 (1997) 31–54.

[30] R. F. Liang, M. R. Mackley, Rheological characterization of the time and strain dependence for polyisobutylene solutions, Journal of Non-Newtonian Fluid Mechanics 52 (1994) 387–405.

[31] A. V. Bazilevskii, V. M. Entov, M. M. Lerner, A. N. Rozhkov, Degradation of polymer solution filaments, Vysokomolekulyarnye Soedineniya Seriya A and Seriya B 39 (1997) 474–482.

[32] M. Stelter, G. Brenn, Validation and application of a novel elongational device for polymer solutions, Journal of Rheology 44 (2000) 595–616.

[33] J. P. Plog, W. M. Kulicke, C. Clasen, Influence of the molar mass distribution on the elongational behaviour of polymer solutions in capillary breakup, Applied Rheology 15 (2005) 28–37.

[34] B. Yesilata, C. Clasen, G. H. McKinley, Nonlinear shear and extensional flow dynamics of wormlike surfactant solutions, Journal of Non-Newtonian Fluid Mechanics 133 (2006) 73–90.

[35] E. Miller, C. Clasen, J. P. Rothstein, The effect of step-stretch parameters on capillary breakup extensional rheology (caber) measurements, Rheologica Acta 48 (2009) 625–639.

[36] C. Clasen, Capillary breakup extensional rheometry of semi-dilute polymer solutions, Korea-Australia Rheology Journal (2010) accepted.

[37] L. E. Rodd, T. P. Scott, J. J. Cooper-White, G. H. McKinley, Capillary break-up rheometry of low-viscosity elastic fluids, Applied Rheology 15 (2005) 12–27.

[38] D. C. Vadillo, T. R. Tuladhar, A. C. Mulji, S. Jung, S. D. Hoath, M. R. Mackley, Evaluation of the inkjet fluid's performance using the "cambridge trimaster" filament stretch and break-up device, Journal of Rheology 54 (2010) 261–282.

[39] P. P. Bhat, S. Appathurai, M. T. Harris, M. Pasquali, G. H. McKinley, O. A. Basaran, Formation of beads-on-a-string structures during breakup of viscoelastic filaments, Nature Physics 6 (2010) 625–631.

[40] A. M. Ardekani, V. Sharma, G. H. McKinley, Dynamics of bead formation, filament thinning and breakup in weakly viscoelastic jets, Journal of Fluid Mechanics accepted (2010).

[41] N. F. Morrison, O. G. Harlen, Viscoelasticity in inkjet printing, Rheologica Acta 49 (2010) 619–632.

[42] S. D. Hoath, I. M. Hutchings, G. D. Martin, T. R. Tuladhar, M. R. Mackley, D. Vadillo, Links between ink rheology, drop-on-demand jet formation, and printability, Journal of Imaging Science and Technology 53 (2009) 8.

[43] B. J. de Gans, P. C. Duineveld, U. S. Schubert, Inkjet printing of polymers: State of the art and future developments, Advanced Materials 16 (2004) 203–213.

[44] L. A. Slobozhanin, J. M. Perales, Stability of liquid bridges between equal disks in an axial gravity-field, Physics of Fluids A-Fluid Dynamics 5 (1993) 1305–1314.

[45] M. P. Brenner, J. R. Lister, H. A. Stone, Pinching threads, singularities and the number 0.0304..., Physics of Fluids 8 (1996) 2827–2836.

[46] D. T. Papageorgiou, On the breakup of viscous-liquid threads, Physics of Fluids 7 (1995) 1529–1544.

[47] G. H. McKinley, A. Tripathi, How to extract the Newtonian viscosity from capillary breakup measurements in a filament rheometer, Journal of Rheology 44 (2000) 653–670.

[48] S. H. Spiegelberg, D. C. Ables, G. H. McKinley, The role of end-effects on measurements of extensional viscosity in filament stretching rheometers, Journal of Non-Newtonian Fluid Mechanics 64 (1996) 229–267.

[49] J. Eggers, Nonlinear dynamics and breakup of free-surface flows, Reviews of Modern Physics 69 (1997) 865–929.

[50] R. F. Day, E. J. Hinch, J. R. Lister, Self-similar capillary pinchoff of an inviscid fluid, Physical Review Letters 80 (1998) 704–707.

[51] A. U. Chen, P. K. Notz, O. A. Basaran, Computational and experimental analysis of pinch-off and scaling, Physical Review Letters 88 (2002) 174501.

[52] A. Rothert, R. Richter, I. Rehberg, Transition from symmetric to asymmetric scaling function before drop pinch-off, Physical Review Letters 87 (2001) 084501.

[53] T. A. Kowalewski, On the separation of droplets from a liquid jet, Fluid Dynamics Research 17 (1996) 121–145.

[54] C. Clasen, J. Eggers, J. L. Fontelos, G. H. McKinley, The beads-on-string structure of viscoelastic threads, Journal of Fluid Mechanics 556 (2006) 283–308.

[55] J. Li, M. A. Fontelos, Drop dynamics on the beads-on-string structure for viscoelastic jets: A numerical study, Physics of Fluids 15 (2003) 922.

[56] M. S. N. Oliveira, R. Yeh, G. H. McKinley, Iterated stretching, extensional rheology and formation of beads-on-a-string structures in polymer solutions, Journal of Non-Newtonian Fluid Mechanics 137 (2006) 137–148.

[57] O. G. Harlen, Jet break-up of polymer solutions in inkjet printing, in: http://www.ima.umn.edu/2009-2010/W10.12-16.09/.

837 [58] C. Clasen, J. Bico, V. M. Entov, G. H. McKinley, 'Gobbling drops':
838 the jetting-dripping transition in flows of polymer solutions, Journal of
839 Fluid Mechanics 636 (2009) 5–40.

840 [59] H. C. Oettinger, Stochastic Processes in Polymeric Liquids, Springer
841 Verlag, Berlin, 1996.

842 [60] J. Brandrup, E. H. Immergut, Polymer Handbook, John Wiley & Sons,
843 New York, 4th edition, 1999.

844 [61] G. H. McKinley, personal communication, 2002.